



Electronic properties of bismuth nanostructuresChristian König ¹, James C. Greer ^{2,*} and Stephen Fahy^{1,3}¹*Tyndall National Institute, University College Cork, Lee Maltings, Cork T12 R5CP, Ireland*²*Nottingham Ningbo New Material Institute and Department of Electrical and Electronic Engineering, University of Nottingham Ningbo China, 199 Taikang East Road, Ningbo 315100, China*³*Department of Physics, University College Cork, College Road, Cork T12 K8AF, Ireland*

(Received 16 April 2021; accepted 7 July 2021; published 30 July 2021)

The passivation of thin Bi(1 1 1) films with hydrogen and oxide capping layers is investigated from first principles. Considering termination-related changes of the crystal structure, we show how the bands and density of states are affected. In the context of the much-discussed semimetal-to-semiconductor transition and the band topology of the bulk material, we consider the effects of confinement in the whole Brillouin zone and go beyond standard density functional theory by including many-body interactions via the G_0W_0 approximation. The conductivity of unterminated films is calculated via the Boltzmann transport equation using the simple constant relaxation-time approximation and compared to experimental observations that have suggested a two-channel model.

DOI: [10.1103/PhysRevB.104.045432](https://doi.org/10.1103/PhysRevB.104.045432)**I. INTRODUCTION**

The electronic properties of the semimetal bismuth have been subject to intense investigation. The bulk material has a low density of states at the Fermi level, which originates from the indirect overlap in the range of 30 meV to 40 meV [1–5] between the valence band at T and the conduction band at L. The direct band gap is located at the L point and even smaller with a value of only about 10 meV to 15 meV [1,3,5–8]. These delicate features make the material interesting to study but on the other hand also challenging to describe with standard electronic structure methods. Figure 1 shows the crystal structure and electronic structure of the bulk.

Bismuth nanostructures offer a means to probe and manipulate material properties and thus are interesting both from physics and application points of view. Experimental studies have in particular investigated films ranging from the micrometer to the nanometer range. The small effective masses of the charge carriers at the Fermi level lead to confinement effects, which can increase the energy difference between the valence and conduction bands (see, e.g., Refs. [10–14]) and a semimetal-to-semiconductor transition in the nanometer thickness regime has been anticipated and studied by many groups, see, e.g., Refs. [15–19]. Although the transition into the semiconducting regime offers great potential for applications [20,21], it is still subject to an ongoing debate and the growing importance of surface states with increasing surface-to-volume ratio in very thin films has to be considered. The surface state conductivity of Bi(1 1 1) films has been found to be particularly large and in recent years various transport measurements [22–28] and magnetotransport measurements [29–31] suggested that the conductivity of thin films is com-

posed of two channels, i.e., a semiconducting and a metallic contribution, ascribed to the film interior and surface. The passivation of the surface states surprisingly has not been studied to the same extent.

It has been noted, e.g., in Refs. [25,28,30,31], that although the two-channel model is quite successful in describing the measurements, the surface and core regions can not be considered to be completely decoupled. In particular, Ishida [12] showed that the surface states at the $\bar{\Gamma}$ and \bar{M} point extend considerably into the core of the film. Accordingly, the effect of quantum confinement is most pronounced in these regions. The surface states of the films also play a significant role in the discussion of the topological properties of bismuth and their manifestation in two-dimensional films affected by quantum confinement, see, e.g., Ref. [32]. Three-dimensional topologically nontrivial materials have surface states, which are immune to passivation [33].

Various methods have been used in order to obtain the band structure of bismuth although not all of them are easily transferable to nanostructures. The tight-binding model developed by Liu and Allen [34] is commonly used in the literature and aims to reproduce the bulk features around the Fermi level. To do so, interactions up to the third-nearest neighbors had to be included. As pointed out in Refs. [35–37], minimal changes in the model produce basically the same features but induce a topological phase transition. In addition to the uncertainty related to the model (or any other electronic structure method for that matter), another disadvantage of the tight-binding model is that surfaces, which naturally occur in nanostructures are not well described. Therefore, additional surface hopping terms like in Ref. [38] may have to be introduced. Specifically, a simple truncation of the bulk model leads to a crossing of the surface states of Bi(1 1 1) [37], which are important in nanostructures, e.g., for the overall density of states in thin films. Furthermore, tight-binding models are not easily transferable

*Corresponding author: Jim.Greer@nottingham.edu.cn

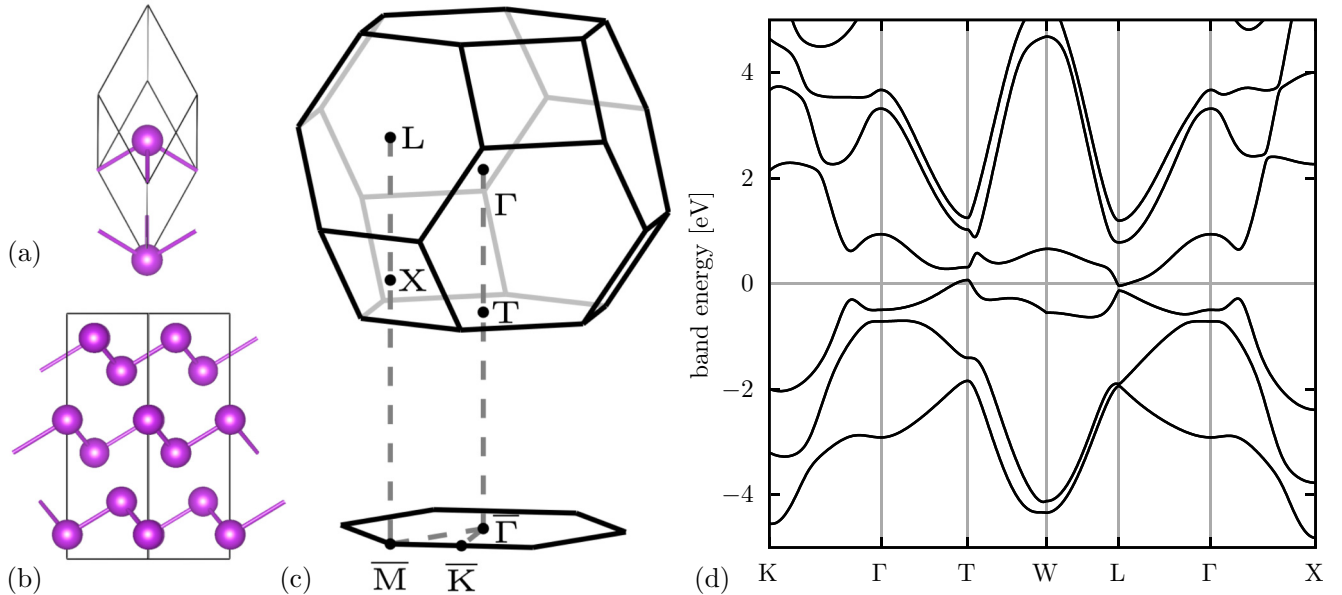


FIG. 1. (a) Rhombohedral Bi unit cell. The second basis atom is slightly displaced from the center of the cell. Therefore, bismuth forms bilayers, which are clearly visible in (b) where we show a side view of the hexagonal supercell (black lines, contains only six atoms). The bilayers lie perpendicular to the $[1\ 1\ 1]$ direction. (c) Brillouin zone of the unit cell with the main high-symmetry points and their projection onto the two-dimensional hexagonal Brillouin zone of the Bi(1 1 1) surface. (d) Band structure of the bulk as calculated with density functional theory. All bands are doubly degenerate due to inversion and time-reversal symmetry (Kramers degeneracy theorem). For more details on the structure we refer to Ref. [9].

and predictions for different types of surface terminations are not possible, making the method not ideal for nanostructures.

Density functional theory (DFT) is a ground state theory and well suited to predict the structure of materials from first principles. However, the electronic states are not accurate by construction, with the exception of the highest valence state, which is the ionization energy [39,40]. The many-body problem is only approximated with the exchange-correlation functional and the states are only meant to reproduce the true charge density for the system (rather than quasiparticle energies) [39]. Nevertheless, DFT is often used for calculations of the band structure. As it turns out, the results often are reasonable with exception of the notorious underestimation of the band gap. Therefore, with respect to the Bi tight-binding model, DFT suffers from similar issues since an artificial inversion of the small L gap might occur, with consequences for the topology of the bulk material.

The problems of the methods described above can be minimized by means of the GW method, which corrects the state energies as calculated with DFT by replacing the exchange-correlation functional with the calculation of the self-energy, see, e.g., Ref. [39]. Thus, the interaction and screening between the electrons is more accurately described, leading in general to more reliable results and a much better agreement between the calculated band gap and its experimental value [39]. Naturally, the computational cost increases accordingly.

In the following we use density functional theory with complementary G_0W_0 calculations in order to investigate if the surface states in thin Bi(1 1 1) films can be passivated. We furthermore discuss the effects of confinement in the films as calculated with both methods as well as the consequences for the band gap and conductivity.

II. COMPUTATIONAL DETAILS

The plane-wave code QUANTUM ESPRESSO [41,42] was used for all density functional theory calculations. The generalized gradient approximation (GGA) as formulated by Perdew, Burke, and Ernzerhof [43] was employed using fully-relativistic and norm-conserving SG15 pseudopotentials [44–46]. We note that spin-orbit coupling is essential for a good description of the electronic structure of bismuth and is taken into account in every step of our calculations, including the G_0W_0 correction of the state energies for which we used YAMBO [47,48].

In the following we discuss the properties of thin bismuth films with different geometries. To start with, we show the effect of confinement on the surface states of Bi(1 1 1) films as calculated with DFT. In order to allow for a comparison with the bulk and previous calculations, we used the experimental lattice parameters from Ref. [49] measured at roughly 300 K, which are also used in Ref. [1]. A kinetic-energy cutoff of 50 Ry and a kinetic charge-density cutoff of 200 Ry proved to be sufficient to very accurately obtain the state energies on a $6 \times 6 \times 1$ k -point grid. The vacuum was set to 20 Å, which is more than sufficient to suppress interactions between the periodic images of the slab. A bulk calculation in a hexagonal supercell was done for the projected bulk states. The results are compared to those of a G_0W_0 calculation.

In addition to that, the effect of surface termination on the structures previously described in Ref. [50] with regards to a passivation of the surface states is discussed. These structures were optimized (under constraints) so that the remaining forces do not exceed 5×10^{-2} eV/Å. While accurate forces require a kinetic-energy cutoff of up to 100 Ry, the state

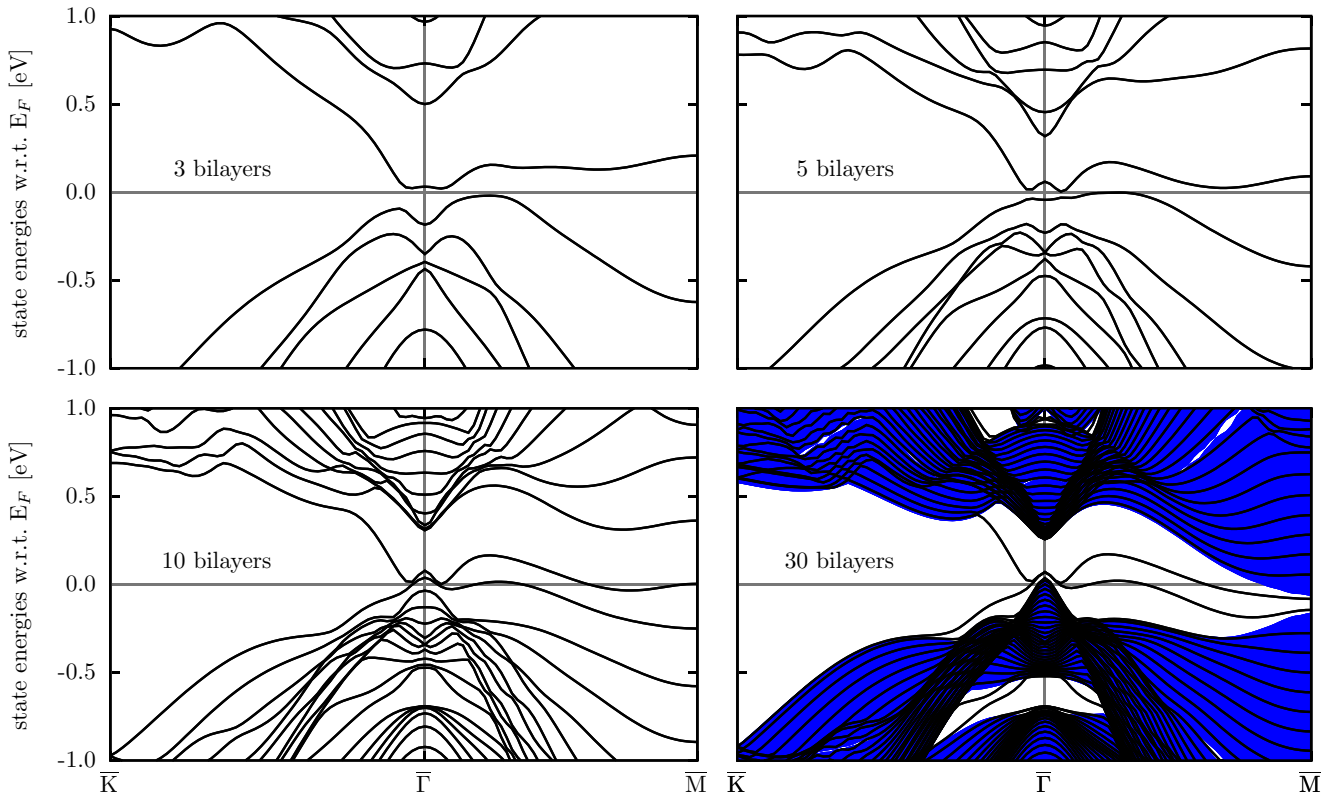


FIG. 2. DFT band structures for films with 3, 5, 10, and 30 bilayers (i.e., 1.0 nm, 1.7 nm, 3.7 nm, and 11.6 nm) thickness. The slabs were cut from the bulk with experimental geometry; no further relaxation was allowed. The number of quantum-well states grows with increasing thickness, approaching the bulk limit. By the same token, the splitting of the valence and conduction bands is strong only in thin films and gradually decreases. In line with Ref. [12], mainly $\bar{\Gamma}$ and in particular \bar{M} are affected by confinement. For 30 bilayers we also show the projected bulk band structure. Here the effect of confinement at $\bar{\Gamma}$ is small, so that the band edges give a clear energy reference where we can align the projected band structure to. Since the surface states do not connect to the valence and conduction bands at \bar{M} any more, it follows that the DFT calculation predicts a trivial band topology for bulk bismuth, see, e.g., Fig. 3(c) in Ref. [36]. At $\bar{\Gamma}$, the surface states are degenerate but do not connect to the bulk valence bands. This is in contrast to Refs. [13,37,58], presumably due to the lack of a clear energy reference as only the Fermi level is used for the relative alignment of the bands to the projected bulk states.

energies converge faster, which reduces the computational cost, in particular regarding the G_0W_0 calculations. Therefore, in general, for all structures a cutoff of 60 Ry or more was used for the calculation of DFT states, which can serve as input for G_0W_0 .

We use the random phase and plasmon pole approximations implemented in YAMBO. Notably, G_0W_0 requires more k points than DFT to converge. In order to ensure reliable results, our calculations use up to $30 \times 30 \times 1$ k points. For even better accuracy of the \bar{M} gap we employed an extrapolation scheme. Further details are given below. Furthermore, a Coulomb cutoff [51] has to be used in YAMBO to completely avoid the interaction between the slab and its periodic images. The particular implementation requires even more vacuum than the DFT calculations and the overall cell height has to be more than twice the thickness of the slab. The combination of both effects, and of course the total number of electrons in the system, limits the maximum film thickness for which the many-body corrections can be calculated.

Since YAMBO only determines the quasiparticle energies on a uniform grid of k points, an interpolation method has to be used to plot the band structure. An interpolation to a fine grid in k space is also useful in order to calculate the conductivity.

Thus, we interpolate the bands with BOLTZTRAP2 [52,53] via a smooth Fourier interpolation scheme [54–57], which exactly reproduces the input data. The density of states and conductivity are subsequently calculated by a bespoke code developed in-house.

III. SURFACE STATES ON THE Bi(1 1 1) SURFACE

Figure 2 shows the band structure of thin unterminated Bi(1 1 1) slabs with a thickness between 3 and 30 bilayers. By comparison with the projected band structure of the bulk (shaded region in the figure), the two surface bands can be identified at the Fermi level as they appear in the projected bulk gap. In fact, each of the bands is degenerate with another band and the two states correspond to the two surfaces of the slab. Only in a semi-infinite bulk, there is no second surface and therefore no degeneracy so that two spin-split bands remain on the surface. The states in a slab are subject to quantum confinement perpendicular to the surface so that the energy splitting between the valence and conduction states increases with respect to the bulk. Since the direct band overlap of Bi is small, a semimetal-to-semiconductor transition has been expected even for relatively thick films (between 23 nm to

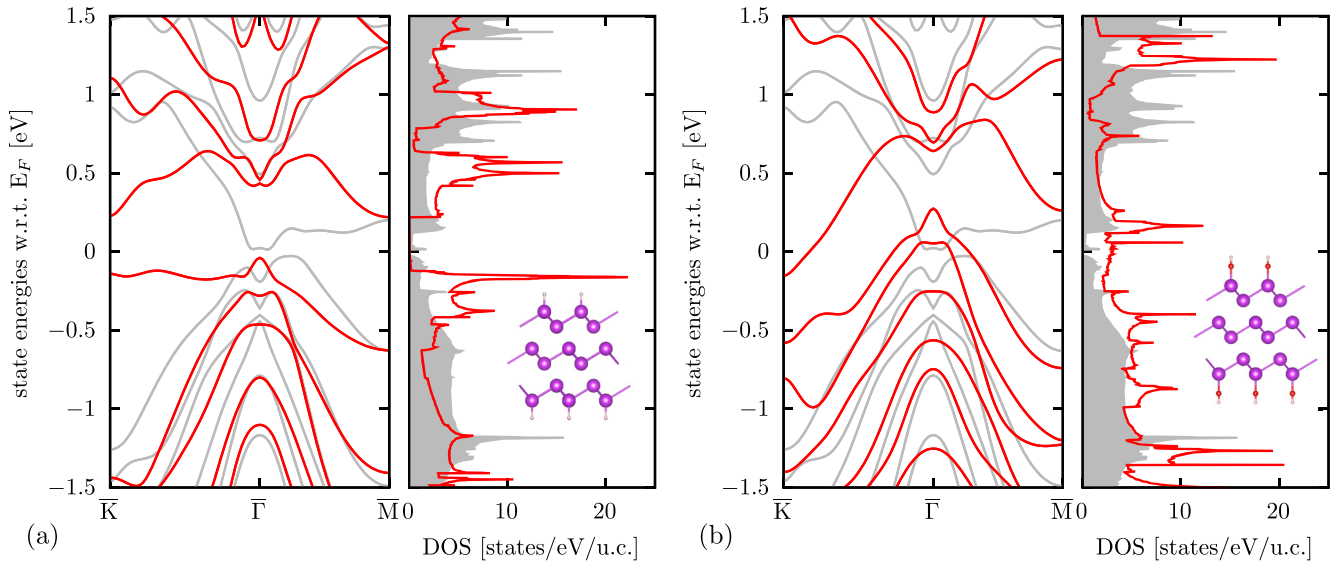


FIG. 3. DFT: (a) Band structure and DOS of a hydrogen terminated slab. For simplicity, the slab was kept in the experimental geometry of the bulk and only the H atoms were relaxed. We also show the data for the unterminated slab in gray. Clearly, the points $\bar{\Gamma}$ and \bar{K} are affected by the surface termination. At $\bar{\Gamma}$, the conduction bands are pushed to higher energies, which increases the overall distance between the occupied and unoccupied states in the Brillouin zone. The previously very large local gap at \bar{K} is reduced while the \bar{M} point is only marginally affected. In this artificial but controlled setting, we observe a passivation of the surface, which results in a band gap of 259 meV. (b) Results for the hydroxyl termination. In comparison to (a), the main difference is the \bar{K} point where the lowest conduction band (effectively one of the two surface bands) drops below the Fermi level so that the system becomes even more metallic. This is clearly reflected in the DOS.

32 nm) [9,15,17–19]. Nevertheless, the experimental observations made are not without ambiguity and the transition is still subject to debate.

It is clear from Fig. 2 that the effect of confinement is most prominent at \bar{K} , $\bar{\Gamma}$, and particularly \bar{M} . The states between $\bar{\Gamma}$ and \bar{M} remain relatively close to the Fermi level. For details we refer to Ref. [12]. Overall, the expected onset of a semiconducting phase with a large band gap is not in agreement with the predictions of density functional theory. We can only see a very small gap for three bilayers or about 1 nm thickness, which is also sensitive to further relaxations away from the experimental bulk lattice. In fact, the expectations formulated above rely on an idealized picture of quantum confinement as a perturbation to the bulk. The fact that broken bonds may give rise to metallic states at the surface is not considered. In other words, it is assumed that the surface states are removed from the band structure by passivation. This passivation, e.g., with a native oxide, may be required in Bi films to open the band gap (see also Ref. [22]). In the following we investigate if a hydrogen, hydroxyl or Bi_2O_3 termination as presented in Ref. [50] can achieve passivation of the surface bands.

The discussion will be divided into two sections. First of all, we start by using the experimental bulk geometry for a three bilayer thick film. Thus we can clearly isolate the effect of the surface termination without any side effects, e.g., further relaxation of the films. Each side of the slab will be terminated with hydrogen or hydroxyl, which is allowed to relax on the surface. For the oxide termination, a five bilayer slab is used where the upper and lower bilayers are oxidized and relaxed. Afterwards, we consider further relaxation of the structures and apply strain equivalent to lattice matched growth of $\text{Bi}(1\ 1\ 1)$ on a $\text{Si}(1\ 1\ 1)-7 \times 7$ substrate.

Figure 3 shows the bands and density of states (DOS) of the $-\text{H}$ and $-\text{OH}$ terminated structures and compares the results to the unterminated slab. We can see that the hydrogen termination does reduce the DOS at the Fermi level by pushing the lowest conduction band states at $\bar{\Gamma}$ to higher binding energies. In turn, the splitting at \bar{K} is reduced—but not enough to close the gap. As we will show subsequently, further relaxation of the structure will close the gap again. The hydroxyl termination has a similar effect on the band structure, but the changes at \bar{K} are even more pronounced. The first conduction band crosses the Fermi level and closes the global gap due to an overlap with the valence bands at $\bar{\Gamma}$.

The oxide termination in Fig. 4(a) on the other hand basically does not have any significant effect on the surface states. The equilibrium position of the oxide layers is further away from the Bi core than another Bi bilayer would be. Figure 4(a) shows the band structures of the full terminated slab, the core Bi region, and the isolated oxide layers. Clearly, the surface bands are affected only slightly and there appears not to be enough chemical interaction with the oxide to push the states away from the Fermi level. The band dispersion of the valence bands below -1 eV is to a good approximation just a superposition of the bands of the two subsystems. Since GGA underestimates the bond strengths, we also investigated how the electronic structure is affected if the oxide layers are closer to the surface of the Bi slab. Keeping those Bi atoms of the oxide layers, which are closest to the slab in the position of a new bilayer, the interaction is enhanced slightly. However, rather than passivating the slab, the states at $\bar{\Gamma}$ are affected such that the small band gap is closed completely.

We note that the band gap of our oxide layers (approximately 2.6 eV) is in good agreement with experimental values

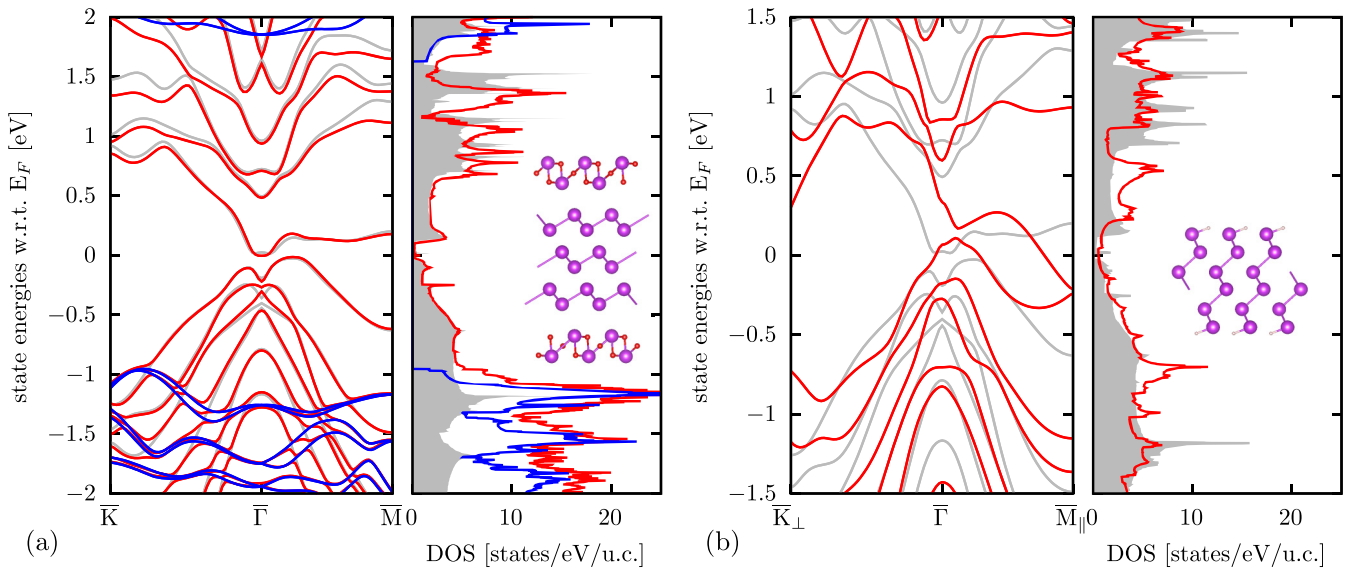


FIG. 4. DFT: (a) Band structure and density of states for the oxide terminated slab in red, the unterminated slab in gray, and the corresponding isolated oxide layers in blue. While the Bi core region was kept in the experimental bulk geometry, the oxide was relaxed on the surface of the film and shows very little interaction with the core. In particular, the surface bands at the Fermi level are not affected and the band structure is basically a superposition of those of the subsystems. Thus, the oxide termination has no passivating effect on the surface states. The bands of the relaxed hydrogen terminated structure are shown in (b) where the in-plane lattice constant was kept fixed. The reorientation of the film has a significant impact on the electronic structure. The C_3 symmetry is lost, so that the \bar{M} points (and \bar{K} points) are no longer equivalent. Thus, we have chosen a path, which is perpendicular and parallel to the characteristic direction of the system, given by the orientation of the surface bonds. The valence and conduction bands overlap in the direction of the Bi-H bonds and therefore the system remains semimetallic.

for α - Bi_2O_3 , which is the most common and stable oxide phase [59–62]. The native oxide on the films in Ref. [21] was found to be Bi_2O_3 . Five different phases of bulk Bi_2O_3 are known and the native oxide layer may, as is shown in Refs. [59–61] for Bi_2O_3 films, consist of a mixture of these phases (or even amorphous regions and regions with different stoichiometry, also depending on the preparation conditions). Values of 2.15 eV and 2.60 eV for the indirect (thermal and optical) band gap in α - Bi_2O_3 and 2.91 eV for the direct (optical) gap were reported in Ref. [63]. However, there is considerable variation to be expected (2.3 eV to 3.3 eV for the optical gap in the oxide films, 2.3 eV for α - Bi_2O_3 , and about 2 eV for amorphous films in Ref. [61]). The structure of the native oxide and the layered oxide model may not coincide with the bulk phases, so that the electronic structure is modified. Confinement may also further change the band gap in the thin oxide layers. Nevertheless, overall the model appears to describe the oxide layers reasonably well¹.

After this simplified investigation, there are two additional factors, which have to be considered for the realistic description of the films. First of all, the slabs might relax further, in particular perpendicular to the substrate. Chemical interaction with the goal of passivating the surface will have an impact on the overall structure. This has been discussed in Ref. [50] for hydrogen and hydroxyl termination, which changed the orientation of the whole film for sufficiently small thickness. A stronger covalent bonding between film and oxide than

observed here for our model can be expected to lead to a change in the orientation of the crystal close to the surface. Furthermore, lattice strain due to the growth on a mismatched substrate such as $\text{Si}(111)-7 \times 7$ has to be considered.

In any case, we require a relaxation of the full structure with respect to the experimental bulk lattice. We note that the weak forces between the layers in combination with the high number of atomic coordinates makes it difficult for common relaxation algorithms to find the true global energy minimum. To start with, Fig. 4(b) shows the hydrogen terminated film after relaxation where the in-plane lattice constant was kept fixed at 4.546 Å. We observe the expected reorientation of the film induced by the covalent bonds at the surface, which has a significant impact on the electronic structure of the film. Since the rotational symmetry of the previously hexagonal surface is lost, we have chosen those \bar{K} and \bar{M} points for the band structure plot, which are perpendicular and parallel with the in-plane orientation of the Bi-H bond. The overlap between the valence and conduction band has increased significantly due to the changes at the \bar{M} point and the film has become even more metallic. Therefore, it is not realistic to assume that a hydrogen termination would lead to the passivation seen in the unrelaxed geometry shown in Fig. 3(a).

There are some further intricacies of the electronic structure related to the equilibrium geometry of the film. Figure 5(a) shows the band structure and DOS of a bismuth film with the same in-plane lattice constant as the previously discussed films. The remaining parameters that determine the crystal structure were optimized for a minimum bulk energy. Since GGA underestimates the bond strengths, the interlayer distance increases. As a consequence, as we have discussed

¹The band gap is wide enough so that the coupling of the oxide to the Bi states at the Fermi level is small.

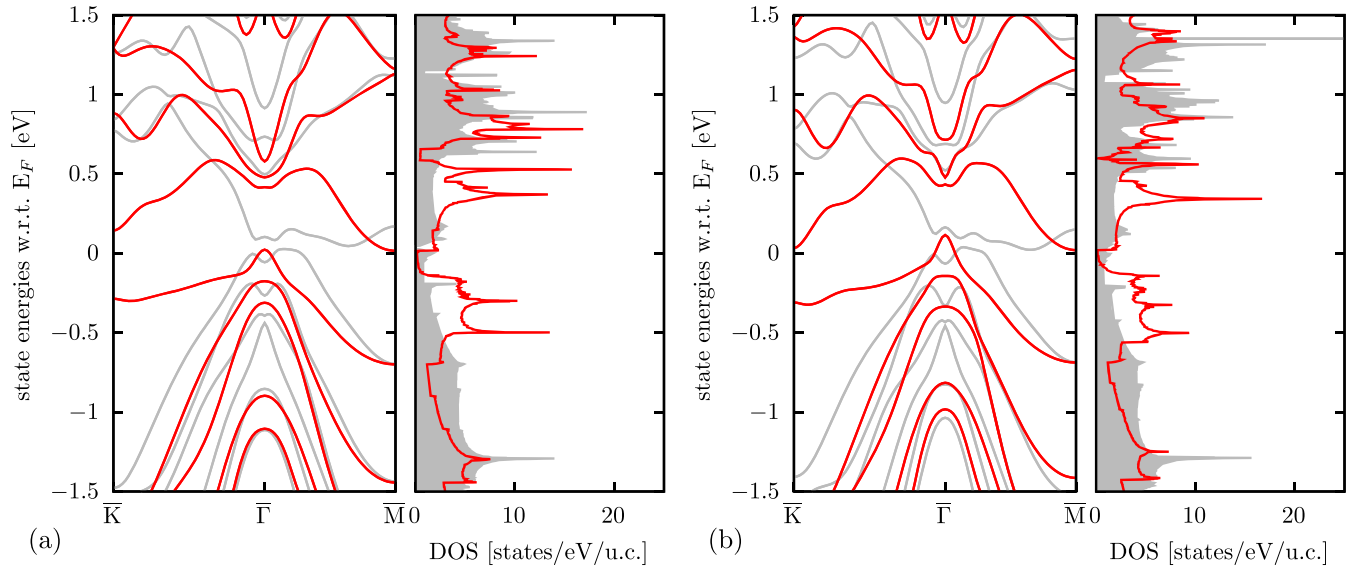


FIG. 5. DFT: The figure shows the effects of relaxation and strain on three bilayer thick films. The results for the unterminated slabs are shown in gray while the red curves correspond to those with termination. The slab in (a) was cut from a bulk lattice where the out-of-plane lattice constant c_h and atomic positions were optimized via a minimum energy fit (GGA). Effectively the inter-bilayer distance increased while a_h was not changed with respect to the previous calculations. As a consequence, the T-L overlap increases in the unterminated slab (dip in the surface state between $\bar{\Gamma}$ and \bar{M}) although the splitting due to confinement is much stronger at \bar{M} . However, compared to the previous crystal structure, the overlap at \bar{M} also increases if H is attached to the surface and the DOS remains semimetallic even with termination. Panel (b) corresponds to a thin film on a Si(1 1 1)- 7×7 substrate, i.e., 1.3% in-plane compressive strain. In order to avoid issues with the interlayer distance, we deduced c_h by assuming constant volume. The atomic positions in the bulk were also optimized via a fit. We observe an effect similar to (a) with increasing indirect band overlap and an almost identical semimetallic density of states at the Fermi level. However, in contrast to (a), this not due to the deficiencies of DFT regarding the equilibrium structure.

previously in Ref. [64], the indirect band overlap between T and L increases². These high-symmetry points of the bulk project to the $\bar{\Gamma}$ and \bar{M} point of the slab, see Fig. 1(c). Indeed, compared to Fig. 3(a), the surface state of the unterminated slab (drawn in gray) between these two points drops in Fig. 5(a) to lower energies and closes the gap of the unterminated slab. Directly at \bar{M} , the effect of confinement is much stronger and pushes the bands apart. Hydrogen was then used to passivate the surface and only the H atoms were relaxed. The corresponding band structure of the terminated slab is drawn in red. Notably, in contrast to the case of experimental lattice geometry, the first conduction state at \bar{M} now drops in energy, leading to a semimetallic density of states.

Next, we consider the strain, which a Si(1 1 1)- 7×7 substrate exerts on a thin Bi film. The strain in films of this thickness has been reported to be -1.3% so that the bismuth film matches with the silicon substrate with six unit cells of the hexagonal lattice [67–70]. In order to avoid any issues related to the bilayer distance as predicted by the GGA, we apply the strain to the in-plane lattice parameter a_h and adjust the out-of-plane parameter c_h accordingly so that the cell volume is preserved; the coordinates of the basis atoms were optimized for the bulk. The results are shown in Fig. 5(b). Again, the gray bands correspond to the unterminated slab for which the results are very similar to Fig. 5(a). Clearly, the

compressive strain in the plane increases the overlap of the valence and conduction bands in line with the discussion in Ref. [64] for the bulk. Introducing bonding hydrogens to both sides of the film (bands drawn in red) does not passivate the surface since the overlap between the valence and conduction bands persists.

We note again that the relaxation and strain effects also affect the unterminated three bilayer slab in Fig. 2 insofar as the small band gap, which is obtained with experimental bulk geometry, closes.

IV. CONFINEMENT: DFT AND G_0W_0

Based on the observations above, the surface states can not realistically be expected to be removed in our DFT calculations³. In-plane compressive strain or a relaxation towards increasing bilayer distance is further detrimental to passivation since the overlap of the valence and conduction bands increases. Therefore, the reported semiconducting behavior of thin films raises the question if density functional theory achieves an adequate description of the confined system. Since the \bar{M} gap is the most sensitive to confinement and also accessible in experiment via angle-resolved photoemission spectroscopy (ARPES), this quantity is a reasonable observable to check.

²At the same time the material is pushed towards the topologically non-trivial state (decreasing L gap).

³Only in the artificial situation where hydrogen is attached to an otherwise unrelaxed slab, the surface states are sufficiently deformed to open a small band gap, but not entirely removed.

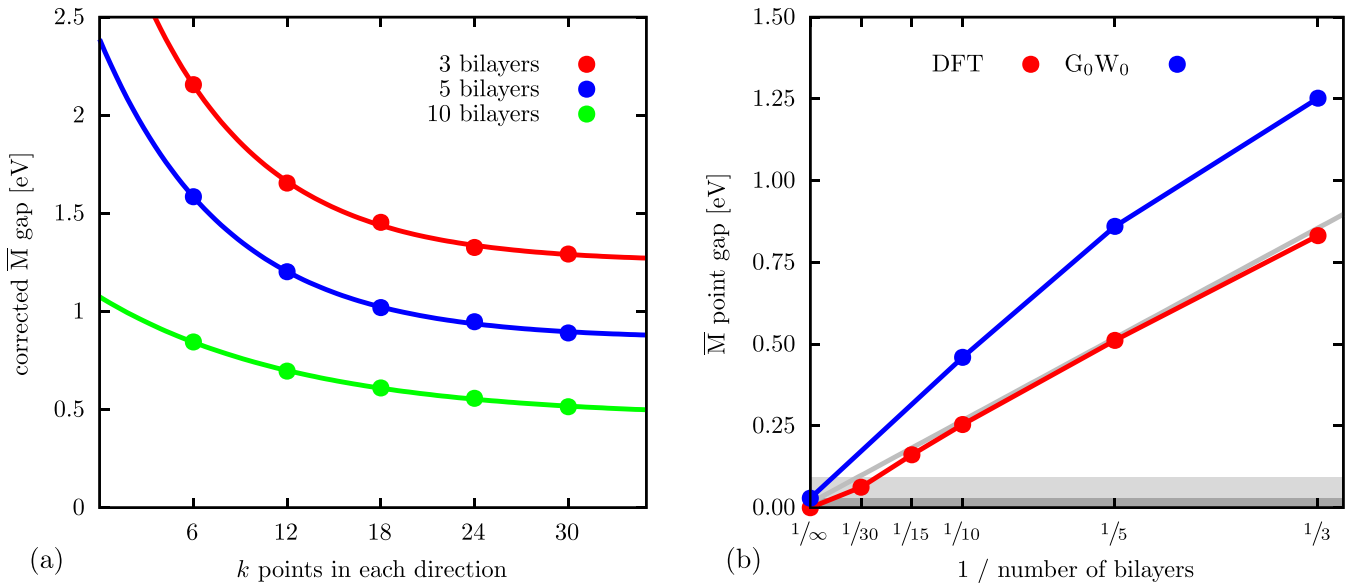


FIG. 6. (a) The direct G_0W_0 \bar{M} gap was fitted as a function of the number of k points in each direction of the Brillouin zone. A decaying exponential was used in order to obtain the converged value. The results are shown in (b) as a function of the reciprocal slab thickness and compared with the DFT values. The light and dark gray areas indicate the L gap of the bulk as calculated in DFT or G_0W_0 , respectively. In DFT, the band topology of bismuth is trivial, which is confirmed by the fact that the value of the \bar{M} gap for 30 bilayers is already smaller than the bulk L gap. In the semi-infinite limit, the surface states still exist but are degenerate as shown in Refs. [12,32,65] and as a result the gap does vanish. In the case of G_0W_0 , we have shown previously [64] that Bi is topologically nontrivial (using the same crystal structure and methods). Thus, one of the surface bands connects to the valence band while the other surface band connects to the conduction band in the semi-infinite limit. The same interpolation was done for the experiments in Refs. [13,66] and the respective data combined with that from Ref. [11] is shown as a gray line. The data contains only films with at least 7 bilayers so that the line is extrapolated to thinner films. Surprisingly, the experimental results match very well with the DFT results whereas G_0W_0 overestimates the \bar{M} gap.

We calculated the \bar{M} gap for films with a thickness between 3 and 30 bilayers, again using the experimental bulk lattice. The results are shown in Fig. 6. There we also compare the DFT results to those of G_0W_0 calculations, which for many materials improve the electronic structure, in particular regarding the energy gaps. As shown in Fig. 6(a), a high number of k points is required in the two-dimensional G_0W_0 calculations and we use an extrapolation scheme in order to obtain well converged results. The limiting factors that determine the maximum film thickness for which calculations are possible are discussed above in Sec. II.

Figure 6(b) shows the same analysis that was applied to the experimental results in Ref. [11] and Refs. [13,66] where the measured \bar{M} gaps were plotted as a function of the reciprocal film thickness and used for an extrapolation to the semi-infinite limit. Since the gap is increased in thin films due to confinement, the relative error is small and the extrapolation is thus more reliable than a direct measurement of the small splitting of the surface bands on the semi-infinite surface, which at the maximum might amount to a value of the order of the bulk L gap. We note that in comparison to the films calculated here, those used in experiment are typically thicker, since these samples are easier to grow with high quality.

A linear dependence of the \bar{M} gap as a function of the reciprocal slab thickness has been found in Ref. [13] over a range of 14 to 202 bilayers, which is explained in Ref. [66] by the Dirac dispersion of the bulk in the direction normal to the film surface; the k_{\perp} of the standing waves are determined by the thickness and by taking into account the phase shifts

at the surface and at the interface to the substrate. Our DFT and G_0W_0 results agree with this observation reasonably well even for a thickness of only a few bilayers. We note that a gap, which is a linear function of the reciprocal thickness has also been taken as an indication of a parabolic confinement potential, e.g., in Ref. [28].

Surprisingly, the DFT results for the \bar{M} gap are already in good agreement with the experimental data while G_0W_0 overestimates the gap substantially. From this perspective, the DFT description of the surface states in thin Bi(1 1 1) films, affected by confinement, appears to be very reasonable. However, the discrepancy of the many-body calculations requires some clarification, particularly since G_0W_0 is known to improve the description of the bulk bands [1,64].

V. FULL MANY-BODY BAND STRUCTURE

Knowing only the size of the \bar{M} gap is not sufficient in the context of a semimetal-to-semiconductor transition and for the interpretation of the conductivity measurements in the literature. Rather, the calculation of many k points in the Brillouin zone equivalent to the full band structure is required. We evaluated the quasiparticle energies on the full 30×30 k -point grid. Figure 7 shows the interpolated band structures for 3-, 5-, and 10-bilayer-thick slabs in bulk-like geometry and compares to the DFT bands.

As we have observed previously, the splitting of the surface states at \bar{M} is enhanced with respect to DFT and the same is

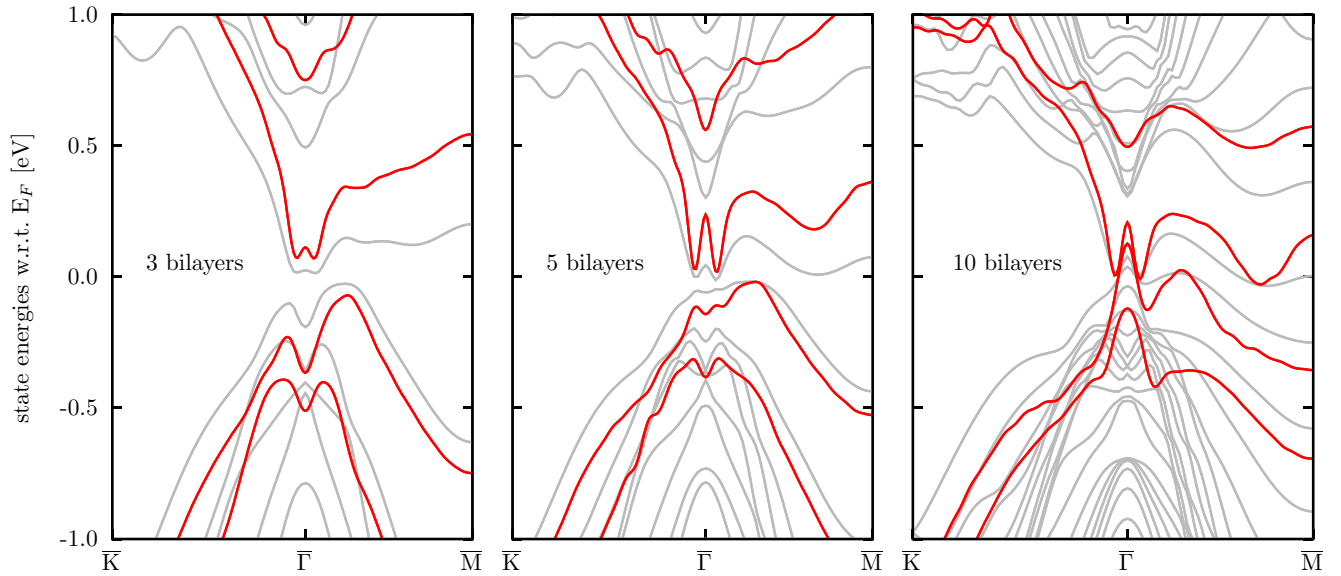


FIG. 7. Band structure of 3-, 5-, and 10-bilayer-thick Bi(1 1 1) films in bulk-like geometry with (red) and without (gray) the many-body corrections. Only the first four valence and conduction bands of the G_0W_0 results were interpolated and plotted for each slab thickness. The interpolation with BOLTZTRAP2 ensures that there are no fitting errors, in particular at \bar{K} , $\bar{\Gamma}$, and \bar{M} , which however causes some Gibbs oscillations on the path between the calculated points. The Fermi level is at 0 eV.

true for \bar{K} . The most interesting however is the behavior in the middle of the Brillouin zone near the $\bar{\Gamma}$ point, where the DFT valence and conduction bands are very close. The many-body corrections split the bands further apart so that for three bilayers a substantial band gap can be observed. Thus, G_0W_0 suggests that quantum confinement alone is sufficient to open a small band gap of about 140 meV in the very thin film and no passivation of the surface states is required. We note however that this gap is smaller than commonly expected for a total thickness of only 1.0 nm. Furthermore, the gap already closes for less than ten bilayers, i.e., 3.7 nm thickness.

Unfortunately, there is not the same amount of data in the literature for other symmetry points than \bar{M} . Based on our observations, the $\bar{\Gamma}$ point of the films and its contribution to the conductivity would be particularly interesting and could offer an explanation for the observed semiconducting properties if the removal of the surface states (i.e. the passivation) indeed fails.

We note that in comparison to the bulk calculation in Ref. [64], the effect of many-body interaction corrections resembles much more that of a scissors operator (see Supplemental Material [71]).

VI. ELECTRONIC TRANSPORT PROPERTIES OF THE FILMS

We used the same interpolation method as described above to obtain the density of states and conductivity σ of the slabs. Since the effect of confinement on the surface states apparently is described reasonably well with density functional theory (at least at \bar{M} where we compared with experimental data), the DFT states were used as basis for the following calculations. Our code uses the tetrahedron method for the calculation of the DOS and the Boltzmann transport equation with the constant relaxation time approximation for σ , similar

to BOLTZTRAP2 [52,53]. The conductivity is then linearly proportional to the constant relaxation time parameter τ . When calculating σ for different temperatures, the occupation of the states changes. Changes of the scattering rates that have been used to distinguish between the metallic surface and the semiconducting bulk channel of the films in experimental data (see, e.g., Ref. [23]) can however not be considered in this simple model.

Figure 8(a) shows the density of states of the thin films. A good description of the surface states is particularly important since they constitute the majority of states at the Fermi level. As we already know, only the three bilayer thick film has a band gap. Notably, films with 10, 15, and 30 bilayers all have approximately the same feature at the Fermi level, which originates from the surface states and thus does not appreciably change if the film thickness is increased further. Upon normalization with the number of bilayers in Fig. 8(c), the density of valence states of 10-, 15-, and 30-bilayer-thick films approaches a converged value, i.e., the bulk limit. A prominent feature at around 100 meV to 200 meV above the Fermi level can be observed for the three bilayer thick film and corresponds to an almost flat surface band. The curvature of this band increases in thicker films but otherwise does not change its position in energy so that the peak spreads over a wider energy range.

The observations above are useful for the interpretation of the conductivity, which is shown in Figs. 8(b) and 8(d) without and with normalization with the slab thickness. First of all, the three and five bilayer thick films are insulating at 0 K. The low-temperature behavior of the sheet conductivity, Fig. 8(b), clearly shows that the critical thickness, below which the surface states require thermal excitation in order to conduct current, lies between five and ten bilayers. In contrast to that, the thicker films all have finite conductivity for low temperatures since the surface states are already partially filled. The

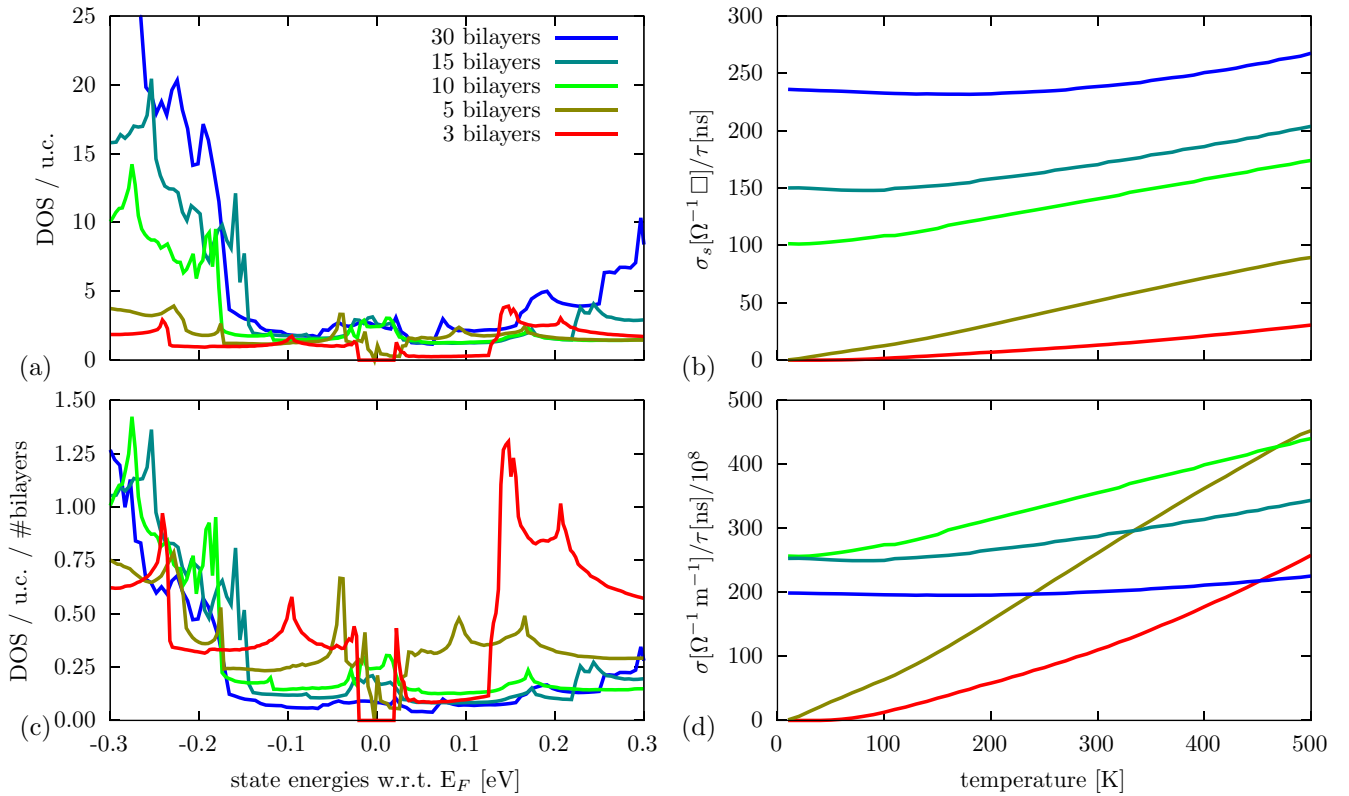


FIG. 8. (a) DFT density of states per two-dimensional unit cell for slabs with different thickness. The band gap of the three bilayer thick film closes for five bilayers. Thicker films all have about the same amount of states near the Fermi level, which is the surface state contribution. (b) shows the corresponding sheet conductivity (depending on the constant relaxation time τ). Slabs with a thickness of ten or more bilayers already conduct for very low temperatures since their surface states cross the Fermi level and are occupied even without thermal excitation. Panel (c) shows the density of states normalized by the slab thickness. The number of valence states per energy in the unit cell is converging quickly towards the bulk limit with increasing thickness. The conductivity in (d) corresponds to (b) divided by the slab thickness. In each case the arithmetic mean of the two in-plane directions is shown.

10 and 15 bilayer films have a very similar conductivity at 0 K and the core of the film remains insulating. The thickest slab with 30 bilayers has an additional low-temperature contribution from the $\bar{\Gamma}$ valence bands.

Similar to Fig. 4 in Ref. [24], when normalized with the number of bilayers, thicker films have a lower conductivity at low temperatures before thermal excitation makes the semiconducting core conduct. Before that, only the surface contributes to the current. However, the films in Fig. 8(d) are thinner than those used in the experiment and we observe the transition from the semiconducting to semimetallic films already at around five bilayers. The G_0W_0 corrected band structures in Fig. 7 suggest the same since the energy gap here also closes at around five bilayers. This threshold agrees well with the measurements in Ref. [22]. Aitani *et al.* [30] report that a transition between surface and bulk dominated transport happens above a film thickness of 16 bilayers.

We expect that more sophisticated models including temperature-dependent scattering will further improve the agreement with the measurements. The changes in the scattering are important to show where the surface contribution is outweighed by the semiconducting core because the metallic states at the surface conduct less at higher temperatures, so that it is possible to clearly distinguish the two channels by

fitting $\sigma(T)$ where required, see, e.g., Ref. [24]. With the simpler approach presented here, we have already identified the onset of conductivity in the unterminated films as a function of thickness in order to compare to the experimentally predicted semimetal-to-semiconductor transition. We also note that for these very thin films an allotropic phase exists, which has a similar effect on the conductivity, see, e.g., Refs. [22,24,67] for more details.

VII. DISCUSSION

In the first part of this paper we have shown how the surface states on thin Bi(1 1 1) slabs react to different kinds of surface termination. The metallic states are not removed but shifted at the three main symmetry points \bar{K} , $\bar{\Gamma}$, and \bar{M} . The importance of the $\bar{\Gamma}$ point for a global band gap as well as relaxation effects (inter-bilayer spacing and reorientations due to surface termination) have been highlighted. We found that the layered-oxide model shows negligible interaction with the film and thus does not passivate the surface. In summary, the passivation of the surface of a three bilayer film was not possible in DFT without additional constraints on the structure.

Subsequently, we have compared the performance of DFT and G_0W_0 regarding an accurate description of the

confinement effects in thin films. The DFT calculations agree very well with experimental results in the literature although the slab thickness is not directly comparable. G_0W_0 , which also reproduces the direct proportionality of the \bar{M} gap with the reciprocal thickness, overestimates the splitting of the bands. This may be a result of substrate-induced strain, which we did not account for above. In a test calculation for the film in Fig. 5(b) we found the \bar{M} gap to increase slightly from 1.25 eV to 1.28 eV upon applying the 1.3% compressive strain. Thus, it is likely that the difference in the \bar{M} gap is rather due to the vicinity of the substrate and the corresponding effect on the screening in the thin film in experiment. Substantial changes in the screening due to a substrate and a concomitant decrease of the band gap has been shown for thin films in Ref. [72]. The good agreement between the experimental \bar{M} gap and the density functional theory results justifies the use of DFT for this passivation study.

Since the bulk material is topologically trivial in DFT, those films, which have the same atomic structure do not have to have topological surface states, which can not be passivated. The situation is different once the many-body corrections are considered. Using the same methods, we have shown previously [64] that bismuth is topologically nontrivial. If bismuth was an insulator, this would mean that metallic surface states exist on the Bi(1 1 1) surface, which connect the valence and conduction bands. Nevertheless, the band structure of the three bilayer thick film in Fig. 7 has a global band gap. There may be two reasons for this kind of behavior. Firstly, as was pointed out in Ref. [36], the overlapping bulk valence and conduction bands can be connected by surface states without crossing the Fermi level. Explicitly, this would mean that both surface states connect to the bulk valence bands at $\bar{\Gamma}$ with a local energy gap between them and further connect to the valence and conduction bands at \bar{M} . Secondly, confinement is a further perturbation to the system. In particular, although it is possible to construct the bulk system corresponding to a strained film, it is not as straightforward to construct such a system taking into account the effects of confinement. Strain is known to drive topological phase transitions and we assume that this is the case for confinement as well, so that the topological constraints do not necessarily remain in very thin films.

With a simple model we have investigated the conductivity of the films and compared σ of the calculated band structures to the popular empirical two-channel model. We observe an onset of the surface state conductivity for a thickness above five bilayers, which agrees well with experimental results. For the interpretation of experimental data for films with a thickness of only a few bilayers, the semiconducting allotropic phase also has to be considered, see, e.g., Refs. [22,24]. A clear distinction between the metallic surface states and the semiconducting core or bulk states, which are populated by thermal excitation, requires the inclusion of more details like electron-phonon scattering.

Realistically, the relaxation time τ depends on the temperature as well as the band energy and position in reciprocal space. Thus, it is also a function of the thickness of the film.

Further relaxations of the thin films that may alter the electronic structure have been neglected completely. Disregarding all these complexities, we can estimate τ for the surface states by comparing with the experimentally obtained surface state conductivity of approximately $1.5 \times 10^{-3} \Omega^{-1}\square$ [22]. The calculated low temperature values for the sheet conductivity between 100 to 250 $\Omega^{-1}\square/\tau$ [ns] correspond to a relaxation time of only 6 fs to 15 fs, which appears to be short and is much smaller than the estimated value of 200 fs, which was reported in Ref. [73]. However, the relaxation time is comparable to the bulk value reported in Ref. [74]. There the electronic lifetime was found to be about the lifetime of the electronic force driving the E_g vibrational mode, which was independent of the excitation energy (corresponding to the band gap for the electron-hole recombination, changing with confinement).

There have been few published studies concerning the effect of termination on the Bi(1 1 1) surface. Liu *et al.* have schematically shown in Ref. [75] how a hydrogen termination changes the band structure. Based on the similarity of their results to Fig. 3(a), we assume that they have also only relaxed the H atoms on the surface but did not allow the whole film to relax. The shown band structure has no substantial band gap. The authors of Ref. [32] investigated the effect of a surface potential, mainly in the context of band topology and the system's response to perturbations. An asymmetric potential was used there to remove some of the interaction between the surface states at \bar{M} and to thus distinguish the topologically trivial and nontrivial phases. The surface potential was then replaced with surface hydrogen bonding to a similar effect as in our calculations and the results of Ref. [75]. Experimentally, arguments for a passivation by oxidation have been found in Ref. [22], although temperature-dependent measurements would be particularly useful in this context, e.g., in order to exclude the full oxidation of the six bilayer thick film. The temperature dependence in the two-channel model and the corresponding measurements only consider unterminated surfaces. The atomistic modeling of the oxide and its interaction with the film as presented above does not suggest a passivation effect. In summary, with the results presented in this paper, we have extended the knowledge on the passivation of thin Bi(1 1 1) films with different kinds of termination and have pointed out the side effects, which occur due to changes in the crystal structure.

ACKNOWLEDGMENTS

This work has been funded by Science Foundation Ireland through the Principal Investigator Award No. 13/IA/1956. The authors wish to acknowledge the Irish Centre for High-End Computing (ICHEC) for the provision of computational facilities and support. Support is also provided by the Nottingham Ningbo New Materials Institute and the National Natural Science Foundation of China with Project Code 61974079. Atomistic structures were visualized with the VESTA software [76].

- [1] I. Aguilera, C. Friedrich, and S. Blügel, Electronic phase transitions of bismuth under strain from relativistic self-consistent GW calculations, *Phys. Rev. B* **91**, 125129 (2015).
- [2] V. S. Édél'man, Investigation of bismuth in a quantizing field, *J. Exp. Theor. Phys.* **41**, 125 (1975).
- [3] R. T. Isaacson and G. A. Williams, Alfvén-wave propagation in solid-state plasmas. III. Quantum oscillations of the Fermi surface of bismuth, *Phys. Rev.* **185**, 682 (1969).
- [4] R. J. Dinger and A. W. Lawson, Cyclotron resonance and the Cohen nonellipsoidal nonparabolic model for bismuth. III. Experimental results, *Phys. Rev. B* **7**, 5215 (1973).
- [5] G. E. Smith, G. A. Baraff, and J. M. Rowell, Effective g factor of electrons and holes in bismuth, *Phys. Rev.* **135**, A1118 (1964).
- [6] M. Maltz and M. S. Dresselhaus, Magnetoreflexion studies in bismuth, *Phys. Rev. B* **2**, 2877 (1970).
- [7] M. P. Vecchi and M. S. Dresselhaus, Temperature dependence of the band parameters of bismuth, *Phys. Rev. B* **10**, 771 (1974).
- [8] R. N. Brown, J. G. Mavroides, and B. Lax, Magnetoreflexion in bismuth, *Phys. Rev.* **129**, 2055 (1963).
- [9] P. Hofmann, The surfaces of bismuth: Structural and electronic properties, *Prog. Surf. Sci.* **81**, 191 (2006).
- [10] T. Hirahara, T. Nagao, I. Matsuda, G. Bihlmayer, E. V. Chulkov, Y. M. Koroteev, P. M. Echenique, M. Saito, and S. Hasegawa, Role of Spin-Orbit Coupling and Hybridization Effects in the Electronic Structure of Ultrathin Bi Films, *Phys. Rev. Lett.* **97**, 146803 (2006).
- [11] T. Hirahara, T. Nagao, I. Matsuda, G. Bihlmayer, E. V. Chulkov, Y. M. Koroteev, and S. Hasegawa, Quantum well states in ultrathin Bi films: Angle-resolved photoemission spectroscopy and first-principles calculations study, *Phys. Rev. B* **75**, 035422 (2007).
- [12] H. Ishida, Decay length of surface-state wave functions on Bi(1 1 1), *J. Phys.: Condens. Matter* **29**, 015002 (2017).
- [13] S. Ito, B. Feng, M. Arita, A. Takayama, R.-Y. Liu, T. Someya, W.-C. Chen, T. Iimori, H. Namatame, M. Taniguchi, C.-M. Cheng, S.-J. Tang, F. Komori, K. Kobayashi, T.-C. Chiang, and I. Matsuda, Proving Nontrivial Topology of Pure Bismuth by Quantum Confinement, *Phys. Rev. Lett.* **117**, 236402 (2016).
- [14] G. Cantele and D. Ninno, Size-dependent structural and electronic properties of Bi(1 1 1) ultrathin nanofilms from first principles, *Phys. Rev. Materials* **1**, 014002 (2017).
- [15] V. N. Lutskii, Features of optical absorption of metallic films in the region where the metal turns into a dielectric, *J. Exp. Theor. Phys. Lett.* **2**, 245 (1965).
- [16] Y. F. Ogrin, V. N. Lutskii, and M. I. Elinson, Observation of quantum size effects in thin bismuth films, *J. Exp. Theor. Phys. Lett.* **3**, 71 (1966).
- [17] V. B. Sandomirskii, Quantum size effect in a semimetal film, *J. Exp. Theor. Phys.* **25**, 101 (1967).
- [18] C. A. Hoffman, J. R. Meyer, F. J. Bartoli, A. Di Venere, X. J. Yi, C. L. Hou, H. C. Wang, J. B. Ketterson, and G. K. Wong, Semimetal-to-semiconductor transition in bismuth thin films, *Phys. Rev. B* **48**, 11431 (1993).
- [19] E. I. Rogacheva, S. G. Lyubchenko, and M. S. Dresselhaus, Semimetal-semiconductor transition in thin Bi films, *Thin Solid Films* **516**, 3411 (2008).
- [20] F. Gity, L. Ansari, M. Lanus, P. Schüffelgen, G. Mussler, D. Grützmacher, and J. C. Greer, Reinventing solid state electronics: Harnessing quantum confinement in bismuth thin films, *Appl. Phys. Lett.* **110**, 093111 (2017).
- [21] F. Gity, L. Ansari, C. König, G. A. Verni, J. D. Holmes, B. Long, M. Lanus, P. Schüffelgen, G. Mussler, D. Grützmacher, and J. C. Greer, Metal-semimetal Schottky diode relying on quantum confinement, *Microelectron. Eng.* **195**, 21 (2018).
- [22] T. Hirahara, I. Matsuda, S. Yamazaki, N. Miyata, S. Hasegawa, and T. Nagao, Large surface-state conductivity in ultrathin Bi films, *Appl. Phys. Lett.* **91**, 202106 (2007).
- [23] F. Pang, X.-J. Liang, Z.-L. Liao, S.-L. Yin, and D.-M. Chen, Origin of the metallic to insulating transition of an epitaxial Bi(1 1 1) film grown on Si(1 1 1), *Chin. Phys. B* **19**, 087201 (2010).
- [24] S. Xiao, D. Wei, and X. Jin, Bi(111) Thin Film with Insulating Interior but Metallic Surfaces, *Phys. Rev. Lett.* **109**, 166805 (2012).
- [25] K. Zhu, L. Wu, X. Gong, S. Xiao, and X. Jin, Quantum transport in the surface states of epitaxial Bi(1 1 1) thin films, *Phys. Rev. B* **94**, 121401(R) (2016).
- [26] T. Hirahara and S. Hasegawa, Comment on "Quantum transport in the surface states of epitaxial Bi(1 1 1) thin films", *Phys. Rev. B* **97**, 207401 (2018).
- [27] K. Zhu, L. Wu, X. Gong, S. Xiao, and X. Jin, Reply to "Comment on 'Quantum transport in the surface states of epitaxial Bi(1 1 1) thin films'", *Phys. Rev. B* **97**, 207402 (2018).
- [28] P. Kröger, D. Abdelbarey, M. Siemens, D. Lükermann, S. Sologub, H. Pfnür, and C. Tegenkamp, Controlling conductivity by quantum well states in ultrathin Bi(111) films, *Phys. Rev. B* **97**, 045403 (2018).
- [29] D. Lükermann, S. Sologub, H. Pfnür, C. Klein, M. Horn-von-Hoegen, and C. Tegenkamp, Effect of adsorbed magnetic and non-magnetic atoms on electronic transport through surfaces with strong spin-orbit coupling, *Mat.-wiss. u. Werkstofftech.* **44**, 210 (2013).
- [30] M. Aitani, T. Hirahara, S. Ichinokura, M. Hanaduka, D. Shin, and S. Hasegawa, *In Situ* Magnetotransport Measurements in Ultrathin Bi films: Evidence for Surface-Bulk Coherent Transport, *Phys. Rev. Lett.* **113**, 206802 (2014).
- [31] D. Abdelbarey, J. Koch, Z. Mamiyev, C. Tegenkamp, and H. Pfnür, Thickness-dependent electronic transport through epitaxial nontrivial Bi quantum films, *Phys. Rev. B* **102**, 115409 (2020).
- [32] T.-R. Chang, Q. Lu, X. Wang, H. Lin, T. Miller, T.-C. Chiang, and G. Bian, Band topology of bismuth quantum films, *Crystals* **9**, 510 (2019).
- [33] M. Z. Hasan and C. L. Kane, Colloquium: Topological insulators, *Rev. Mod. Phys.* **82**, 3045 (2010).
- [34] Y. Liu and R. E. Allen, Electronic structure of the semimetals Bi and Sb, *Phys. Rev. B* **52**, 1566 (1995).
- [35] T. Fukui and Y. Hatsugai, Quantum Spin Hall effect in three dimensional materials: Lattice computation of Z_2 topological invariants and its application to Bi and Sb, *J. Phys. Soc. Jpn.* **76**, 053702 (2007).
- [36] Y. Ohtsubo, L. Perfetti, M. O. Goerbig, P. Le Fèvre, F. Bertran, and A. Taleb-Ibrahimi, Non-trivial surface-band dispersion on Bi(111), *New J. Phys.* **15**, 033041 (2013).
- [37] Y. Ohtsubo and S. Kimura, Topological phase transition of single-crystal Bi based on empirical tight-binding calculations, *New J. Phys.* **18**, 123015 (2016).

- [38] K. Saito, H. Sawahata, T. Komine, and T. Aono, Tight-binding theory of surface spin states on bismuth thin films, *Phys. Rev. B* **93**, 041301(R) (2016).
- [39] F. Aryasetiawan and O. Gunnarsson, The GW method, *Rep. Prog. Phys.* **61**, 237 (1998).
- [40] C.-O. Almbladh and U. von Barth, Exact results for the charge and spin densities, exchange-correlation potentials, and density-functional eigenvalues, *Phys. Rev. B* **31**, 3231 (1985).
- [41] P. Giannozzi, S. Baroni, N. Bonini, M. Calandra, R. Car, C. Cavazzoni, D. Ceresoli, G. L. Chiarotti, M. Cococcioni, I. Dabo *et al.*, QUANTUM ESPRESSO: A modular and open-source software project for quantum simulations of materials, *J. Phys.: Condens. Matter* **21**, 395502 (2009).
- [42] P. Giannozzi, O. Andreussi, T. Brumme, O. Bunau, M. Buongiorno Nardelli, M. Calandra, R. Car, C. Cavazzoni, D. Ceresoli, M. Cococcioni, N. Colonna *et al.*, Advanced capabilities for materials modelling with QUANTUM ESPRESSO, *J. Phys.: Condens. Matter* **29**, 465901 (2017).
- [43] J. P. Perdew, K. Burke, and M. Ernzerhof, Generalized Gradient Approximation made Simple, *Phys. Rev. Lett.* **77**, 3865 (1996).
- [44] D. R. Hamann, Optimized norm-conserving Vanderbilt pseudopotentials, *Phys. Rev. B* **88**, 085117 (2013).
- [45] M. Schlupf and F. Gygi, Optimization algorithm for the generation of ONCV pseudopotentials, *Comput. Phys. Commun.* **196**, 36 (2015).
- [46] P. Scherpelz, M. Govoni, I. Hamada, and G. Galli, Implementation and validation of fully relativistic GW calculations: Spin-orbit coupling in molecules, nanocrystals, and solids, *J. Chem. Theory Comput.* **12**, 3523 (2016).
- [47] A. Marini, C. Hogan, M. Grüning, and D. Varsano, YAMBO: An *ab initio* tool for excited state calculations, *Comput. Phys. Commun.* **180**, 1392 (2009).
- [48] D. Sangalli, A. Ferretti, H. Miranda, C. Attaccalite, I. Marri, E. Cannuccia, P. Melo, M. Marsili, F. Paleari, A. Marrazzo *et al.*, Many-body perturbation theory calculations using the YAMBO code, *J. Phys.: Condens. Matter* **31**, 325902 (2019).
- [49] D. Schiferl and C. S. Barrett, The crystal structure of arsenic at 4.2, 78 and 299° K, *J. Appl. Cryst.* **2**, 30 (1969).
- [50] C. König, S. Fahy, and J. C. Greer, Structural modification of thin Bi(1 1 1) films by passivation and native oxide model, *Phys. Rev. Materials* **3**, 065002 (2019).
- [51] C. A. Rozzi, D. Varsano, A. Marini, E. K. U. Gross, and A. Rubio, Exact Coulomb cutoff technique for supercell calculations, *Phys. Rev. B* **73**, 205119 (2006).
- [52] G. K. H. Madsen and D. J. Singh, BOLTZTRAP. A code for calculating band-structure dependent quantities, *Comput. Phys. Commun.* **175**, 67 (2006).
- [53] G. K. H. Madsen, J. Carrete, and M. J. Verstraete, BOLTZTRAP2, a program for interpolating band structures and calculating semi-classical transport coefficients, *Comput. Phys. Commun.* **231**, 140 (2018).
- [54] R. N. Euwema, D. J. Stukel, T. C. Collins, J. S. DeWitt, and D. G. Shankland, Crystalline interpolation with applications to Brillouin-zone averages and energy-band interpolation, *Phys. Rev.* **178**, 1419 (1969).
- [55] D. G. Shankland, Fourier transformation by smooth interpolation, *Int. J. Quantum Chem.* **5**, 497 (1971).
- [56] D. D. Koelling and J. H. Wood, On the interpolation of eigenvalues and a resultant integration scheme, *J. Comput. Phys.* **67**, 253 (1986).
- [57] W. E. Pickett, H. Krakauer, and P. B. Allen, Smooth Fourier interpolation of periodic functions, *Phys. Rev. B* **38**, 2721 (1988).
- [58] M.-Y. Yao, F. Zhu, C. Q. Han, D. D. Guan, C. Liu, D. Qian, and J.-F. Jia, Topologically nontrivial bismuth(1 1 1) thin films, *Sci. Rep.* **6**, 21326 (2016).
- [59] L. Leontie, M. Caraman, and G. I. Rusu, On the photoconductivity of Bi₂O₃ in thin films, *J. Optoelectron. Adv. Mater.* **2**, 385 (2000).
- [60] L. Leontie, M. Caraman, M. Delibaş, and G. I. Rusu, Optical properties of bismuth trioxide thin films, *Mater. Res. Bull.* **36**, 1629 (2001).
- [61] L. Leontie, M. Caraman, M. Alexe, and C. Harnagea, Structural and optical characteristics of bismuth oxide thin films, *Surf. Sci.* **507-510**, 480 (2002).
- [62] A. Walsh, G. W. Watson, D. J. Payne, R. G. Edgell, J. Guo, P.-A. Glans, T. Learmonth, and K. E. Smith, Electronic structure of the α and δ phases of Bi₂O₃: A combined *ab initio* and x-ray spectroscopy study, *Phys. Rev. B* **73**, 235104 (2006).
- [63] H. Gobrecht, S. Seeck, H.-E. Bergt, A. Märtens, and K. Kossmann, Über Untersuchungen an Wismutoxid-Aufdampfschichten I. Herstellung sowie elektrische und optische Eigenschaften, *Phys. Stat. Sol.* **33**, 599 (1969).
- [64] C. König, J. C. Greer, and S. Fahy, Effect of strain and many-body corrections on the band inversions and topology of bismuth, *Phys. Rev. B* **104**, 035127 (2021).
- [65] K.-H. Jin, H. W. Yeom, and F. Liu, Doping-induced topological phase transition in Bi: The role of quantum electronic stress, *Phys. Rev. B* **101**, 035111 (2020).
- [66] S. Ito, M. Arita, J. Haruyama, B. Feng, W.-C. Chen, H. Namatame, M. Taniguchi, C.-M. Cheng, G. Bian, S.-J. Tang *et al.*, Surface-state Coulomb repulsion accelerates a metal-insulator transition in topological semimetal nanofilms, *Sci. Adv.* **6**, eaaz5015 (2020).
- [67] T. Nagao, J. T. Sadowski, M. Saito, S. Yaginuma, Y. Fujikawa, T. Kogure, T. Ohno, Y. Hasegawa, S. Hasegawa, and T. Sakurai, Nanofilm Allotrope and Phase Transformation of Ultrathin Bi Film on Si(111)-7 × 7, *Phys. Rev. Lett.* **93**, 105501 (2004).
- [68] M. Kammler and M. Horn-von Hoegen, Low energy electron diffraction of epitaxial growth of bismuth on Si(1 1 1), *Surf. Sci.* **576**, 56 (2005).
- [69] T. Nagao, S. Yaginuma, M. Saito, T. Kogure, J. T. Sadowski, T. Ohno, S. Hasegawa, and T. Sakurai, Strong lateral growth and crystallization via two-dimensional allotropic transformation of semi-metal Bi film, *Surf. Sci.* **590**, 247 (2005).
- [70] S. Yaginuma, T. Nagao, J. T. Sadowski, M. Saito, K. Nagaoka, Y. Fujikawa, T. Sakurai, and T. Nakayama, Origin of flat morphology and high crystallinity of ultrathin bismuth films, *Surf. Sci.* **601**, 3593 (2007).
- [71] See Supplemental Material at <http://link.aps.org/supplemental/10.1103/PhysRevB.104.045432> for the effect of the many-body interaction corrections in the context of a scissors operator.
- [72] D. Y. Qiu, F. H. da Jornada, and S. G. Louie, Environmental screening effects in 2D materials: Renormalization of the bandgap, electronic structure, and optical spectra of few-layer black phosphorus, *Nano Lett.* **17**, 4706 (2017).

- [73] H. Du, X. Sun, X. Liu, X. Wu, J. Wang, M. Tian, A. Zhao, Y. Luo, J. Yang, B. Wang, and J. G. Hou, Surface Landau levels and spin states in bismuth (1 1 1) ultrathin films, *Nat. Commun.* **7**, 10814 (2016).
- [74] S. M. O'Mahony, F. Murphy-Armando, É. D. Murray, J. D. Querales-Flores, I. Savić, and S. Fahy, Ultrafast Relaxation of Symmetry-Breaking Photo-Induced Atomic Forces, *Phys. Rev. Lett.* **123**, 087401 (2019).
- [75] Z. Liu, C.-X. Liu, Y.-S. Wu, W.-H. Duan, F. Liu, and J. Wu, Stable Nontrivial Z_2 Topology in Ultrathin Bi(111) Films: A First-Principles Study, *Phys. Rev. Lett.* **107**, 136805 (2011).
- [76] K. Momma and F. Izumi, VESTA 3 for three-dimensional visualization of crystal, volumetric and morphology data, *J. Appl. Crystallogr.* **44**, 1272 (2011).